Progress In Electromagnetics Research Letters, Vol. 27, 161–169, 2011

RANGE DOPPLER ALGORITHM FOR BISTATIC SAR PROCESSING BASED ON THE IMPROVED LOFFELD'S BISTATIC FORMULA

X. Wang[1, *] and D. Y. Zhu[2]

[1]Nanjing University of Posts & Telecommunications, Nanjing 210046, China

[2]Nanjing University of Aeronautics & Astronautics, Nanjing 210016, China

Abstract—This paper presents a new range Doppler algorithm (RDA) for bistatic synthetic aperture radar (SAR) processing in a general configuration based on a bistatic point target reference spectrum: the improved extended Loffeld's bistatic formula (ILBF). The ILBF spectrum is proved to be comparably accurate with the spectrum derived using the method of series reversion (MSR). Based on the expansion of the ILBF spectrum, a new bistatic RDA is developed to process the azimuth invariant and variant bistatic SAR data. Compared with existing bistatic RDA, the new algorithm has a simpler formulation and is able to cope with moderate or high squint bistatic SAR data. The simulated data in the azimuth invariant and variant bistatic configurations are used to validate the new algorithm.

1. INTRODUCTION

Bistatic synthetic aperture radar (SAR) [1–3] is a SAR system [4–6] whose transmitter and receiver are placed on separate platforms. The interest in bistatic SAR systems has rapidly increased in recent years. In the last decade, several approximate bistatic point target spectrums [7–9] and bistatic imaging methods [10–14] have been reported.

Among these approximate spectrums, the Loffeld's bistatic formula (LBF) [7], which is developed earlier, has been used to derive bistatic SAR imaging algorithm [10]. Nevertheless, LBF

Received 26 June 2011, Accepted 3 November 2011, Scheduled 18 November 2011

* Corresponding author: Xin Wang (whxin2002@live.cn).

becomes invalid when the Doppler chirp rates of the transmitter and receiver are significantly different. Using the method of series reversion (MSR), a more precise spectrum is derived in [8]. Based on MSR spectrum, several bistatic imaging algorithms [11, 12] have been proposed. However, MSR spectrum is in the form of a power series, the accuracy of which depends on the order and converge speed of the series. As discussed in [13], LBF becomes invalid in some extreme configurations (i.e., the airborne-spaceborne bistatic SAR). To extend LBF for the general bistatic SAR configuration, Wang et al. introduced a time-bandwidth product (TBP) weighting operation in the derivation of LBF and derived the extended Loffeld's bistatic formula (ELBF) [9]. However, ELBF spectrum is still not accurate enough, which affects its application.

Recently, a new spectrum, i.e., the improved LBF (ILBF), is derived in [14] and proved to be more accurate than the original ELBF. Based on the expansion of the ILBF spectrum about range frequency, a new bistatic range Doppler algorithm (RDA) is developed in this paper to process the azimuth invariant and variant bistatic SAR data. The new algorithm has a simple formulation and is able to cope with moderate or high squint SAR data.

2. THE BISTATIC POINT TARGET REFERENCE SPECTRUM

In bistatic SAR, assuming that radar transmits a linear frequency modulated (LFM) signal with chirp rate k and center frequency f_c, the echo from a single point target can be expressed as

$$S(\tau,t)=w_r\left[\tau-\frac{R_1(t)+R_2(t)}{c}\right]w_a(t-t_c)\exp\left\{j\pi k\left[\tau-\frac{R_1(t)+R_2(t)}{c}\right]^2\right\}$$
$$\exp\left[-j2\pi f_c\frac{R_1(t)+R_2(t)}{c}\right], \quad (1)$$

where τ is the fast (range) time and t the slow (azimuth) time centered at t_c. $R_1(t)$ and $R_2(t)$ are the instantaneous slant ranges from the transmitter and the receiver to the point target, respectively. In (1), $w_r(\tau)$ is the range envelope of the transmission signal and $w_a(t-t_c)$ the azimuth envelope determined by the composite antenna pattern.

With the assumption of $t_c=0$, the range history is written as

$$R(t) = R_1(t)+R_2(t)=\sqrt{R_{10}^2+v_1^2t^2-2R_{10}v_1t\sin\theta_1}$$
$$+\sqrt{R_{20}^2+v_2^2t^2-2R_{20}v_2t\sin\theta_2}, \quad (2)$$

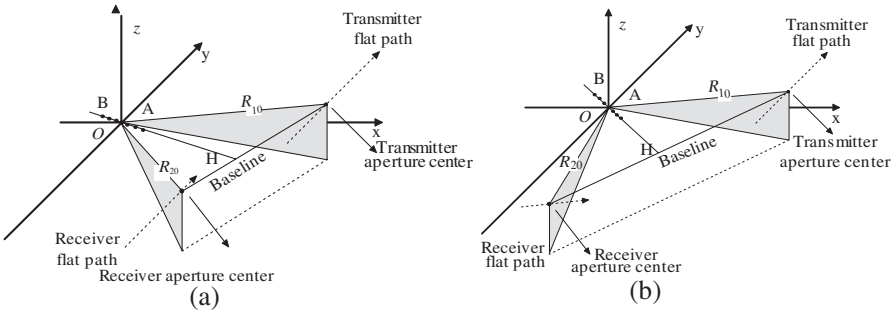

Figure 1. Geometries of the bistatic azimuth (a) invariant and (b) variant SAR in the simulation.

where $R_{10} = R_1(t)|_{t=0}$, $R_{20} = R_2(t)|_{t=0}$, v_1 and v_2 are the velocities of the transmitter and the receiver, respectively. The angles θ_1 and θ_2 in (2) refer to the instantaneous squint angles of the transmitter and the receiver at the composite beam center cross time, respectively.

Performing 2-D Fourier transform on (1), the ILBF [12] can be obtained as

$$S(f_r, f_a) = w_r\left(\frac{f_r}{B}\right) w_a(t_k) \exp\left[-j\varphi(f_r, f_a)\right], \tag{3}$$

where f_r and f_a in (3) denote the range and azimuth frequency, respectively, B the bandwidth of LFM signal, and t_k the stationary phase point. The phase term in (3) is

$$\begin{aligned}\varphi(f_r, f_a) \;=\; & -2\pi\frac{R_{10}\cos\theta_1}{c}F_1 - 2\pi\frac{R_{20}\cos\theta_2}{c}F_2 \\ & -2\pi\left(f_{aT}\frac{R_{10}\sin\theta_1}{v_1} + f_{aR}\frac{R_{20}\sin\theta_2}{v_2}\right) - \pi\frac{f_r^2}{k},\end{aligned} \tag{4}$$

where

$$\begin{aligned}F_1 \;&=\; \sqrt{(f_r+f_c)^2 - \frac{c^2 f_{aT}^2}{v_1^2}}, \\ F_2 \;&=\; \sqrt{(f_r+f_c)^2 - \frac{c^2 f_{aR}^2}{v_2^2}}, \\ f_{aT} \;&=\; k_t\left[f_a - \frac{f_r+f_c}{c}\left(v_1\sin\theta_1 + v_2\sin\theta_2\right)\right] + \frac{f_r+f_c}{c}v_1\sin\theta_1, \\ f_{aR} \;&=\; k_r\left[f_a - \frac{f_r+f_c}{c}\left(v_1\sin\theta_1 + v_2\sin\theta_2\right)\right] + \frac{f_r+f_c}{c}v_2\sin\theta_2,\end{aligned}$$

$$k_t = \frac{v_1^2 \cos\theta_1^2 R_{20}}{v_1^2 \cos\theta_1^2 R_{20} + v_2^2 \cos\theta_2^2 R_{10}},$$

and

$$k_r = \frac{v_2^2 \cos\theta_2^2 R_{10}}{v_1^2 \cos\theta_1^2 R_{20} + v_2^2 \cos\theta_2^2 R_{10}}.$$

3. COMPARABLE PRECISION OF THE ILBF SPECTRUM AND THE MSR SPECTRUM

Among the existing bistatic point target spectrums, MSR spectrum is the most precise, especially in mathematical analysis. To verify the precision of ILBF spectrum, we will expand the phase term of ILBF and compare the expansion with the MSR spectrum.

Expanding the phase term in (4) about the Doppler centriod frequency $f_{ac} = \frac{f_r+f_c}{c}(v_1 \sin\theta_1 + v_2 \sin\theta_2)$, we can obtain

$$\varphi(f_r, f_a) \approx -\pi \frac{f_r^2}{k} - 2\pi \frac{f_r+f_c}{c}(R_{10}+R_{20}) + 2\pi \frac{f_r+f_c}{c} \left\{ \frac{1}{4k_2} \left(\frac{f_a c}{f_r+f_c} + k_1 \right)^2 \right.$$

$$\left. + \frac{k_3}{(2k_2)^3} \left(\frac{f_a c}{f_r+f_c} + k_1 \right)^3 - \left[\left(\frac{A_3^2}{A_2} + \frac{B_3^2}{B_2} \right) \frac{9}{64k_2^4} + \frac{k_4}{(2k_2)^4} \right] \left(\frac{f_a c}{f_r+f_c} + k_1 \right)^4 \right\}, \quad (5)$$

where

$$k_i = \left. \frac{d^i R(t)}{dt^i} \right|_{t=t_c},$$

$$A_i = \left. \frac{d^i R_1(t)}{dt^i} \right|_{t=t_c}, \quad B_i = \left. \frac{d^i R_2(t)}{dt^i} \right|_{t=t_c}, \quad (i = 2, 3).$$

Equation (5) is almost the same as MSR spectrum's phase term that retains the terms in the series up to quartic term. As the fourth order term is usually very small, the little difference will not affect the accuracy of the ILBF spectrum. Hence, the conclusion that the two spectrums are comparably accurate can be obtained. As the MSR spectrum is expressed as a series, the accuracy of which is affected by the expansion order and converge speed of the series used in its derivation. The application of ILBF is more convenient than MSR spectrum.

4. THE NEW BISTATIC RDA

Expanding the phase term in (4) with respect to the range frequency f_r, an explicit form of the ILBF spectrum's phase can be formulated

as

$$\varphi(f_r, f_a) = \varphi_{ar}(f_r, f_a) + \varphi_{src}(f_r, f_a) + \varphi_{rcmc}(f_r, f_a) + \varphi_{az}(f_r, f_a) \quad (6)$$

where

$$\varphi_{ar} = -\pi \frac{f_r^2}{k_r}, \quad (7)$$

$$\begin{aligned}\varphi_{src} = & -\pi f_r^2 \left[R_{10} \cos\theta_1 \frac{c k_t^2 f_a^2}{v_1^2 f_c^4 H_1^4} + R_{20} \cos\theta_2 \frac{c k_r^2 f_a^2}{v_2^2 f_c^4 H_2^4} \right] \\ & -\pi f_r^3 \left\{ R_{10} \cos\theta_1 \frac{c k_t^2 f_a^2}{v_1^2 f_c^5 H_1^5} \left[f_c - \frac{c d_1}{v_2^2} \left(k_r f_a + d_2 \frac{f_c}{c} \right) \right] \right. \\ & \left. + R_{20} \cos\theta_2 \frac{c k_r^2 f_a^2}{v_2^2 f_c^5 H_2^5} \left[f_c - \frac{c d_1}{v_2^2} \left(k_r f_a + d_2 \frac{f_c}{c} \right) \right] \right\}, \end{aligned} \quad (8)$$

$$\begin{aligned}\varphi_{rcmc} = & -2\pi f_r \left[\frac{R_{10} \cos\theta_1}{c H_1} \left(1 - \frac{d_1^2}{v_1^2} - d_1 \frac{k_t f_a c}{v_1^2 f_c} \right) + \frac{R_{20} \cos\theta_2}{c H_2} \right. \\ & \left. \left(1 - \frac{d_2^2}{v_2^2} - d_2 \frac{k_r f_a c}{v_2^2 f_c} \right) + \left(\frac{d_1 R_{10} \sin\theta_1}{c v_1} + \frac{d_2 R_{20} \sin\theta_2}{c v_2} \right) \right], \end{aligned} \quad (9)$$

$$\begin{aligned}\varphi_{az} = & -2\pi \left[\frac{f_c}{c} \frac{R_{10} \cos\theta_1}{H_1} + \frac{f_c}{c} \frac{R_{20} \cos\theta_2}{H_2} + \left(k_t \frac{R_{10} \sin\theta_1}{v_1} \right. \right. \\ & \left. \left. + k_r \frac{R_{20} \sin\theta_2}{v_2} \right) f_a \right], \end{aligned} \quad (10)$$

where

$$\begin{aligned} d_1 &= k_r v_1 \sin\theta_1 - k_t v_2 \sin\theta_2, \\ d_2 &= k_t v_2 \sin\theta_2 - k_r v_1 \sin\theta_1, \\ H_1 &= \sqrt{1 - \frac{c^2 \left(d_1 \frac{f_c}{c} + k_t f_a \right)^2}{f_c^2 v_1^2}}, \\ H_2 &= \sqrt{1 - \frac{c^2 \left(d_2 \frac{f_c}{c} + k_r f_a \right)^2}{f_c^2 v_2^2}}. \end{aligned}$$

With the typical process flow of RDA, the new algorithm can be developed. After range compressed using the phase term in (7), the data is transformed into the 2D domain by an azimuth FFT and range compressed again. The range compressed data is then transformed into the RD domain via a range IFFT and RCM corrected via interpolation according to Equation (9), where a sinc interpolator is used in our simulation in Section 5. Finally, an azimuth matched filter with the

phase term being the negative of (10) is used to azimuth compress the signal and implement the algorithm.

The new bistatic RDA can be used to process the azimuth invariant and variant bistatic SAR data directly. When the transmitter and the receiver platforms move along unparallel paths with different velocities, the algorithm can be used to process the received signal directly. However, the locations of the focused point targets in the image in the azimuth variant configuration will be different from that in the azimuth invariant case.

5. SIMULATION

Two bistatic configurations (i.e., azimuth invariant and variant cases) will be simulated to validate the new bistatic RDA. Table 1 lists the parameters. Seven point targets with interval of 200 m along the bistatic bisector line are used in the simulation, where the geometries in the azimuth invariant and variant cases are depicted in Fig. 1(a) and Fig. 1(b), respectively. Point targets in the simulation are depicted along the bistatic bisector line OH in the figures, where the point target A lies at the scene center, and the point target B lies 600 m away from the scene center.

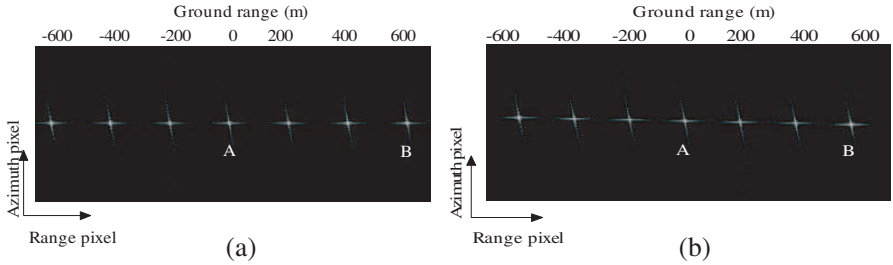

Figure 2. Images in azimuth (a) invariant and (b) variant case.

Table 1. Simulation parameters.

	Azimuth invariant		Azimuth variant	
	Transmitter	Receiver	Transmitter	Receiver
Velocity in x direction	190 m/s	190 m/s	190 m/s	155.8 m/s
Velocity in y direction	0 m/s	0 m/s	0 m/s	60.0 m/s
Squint angle	30°	30°	30°	30°
Bistatic centriod range	15237 m		13010 m	
Range bandwidth	80 MHz		80 MHz	
Baseline	10519 m		10519 m	

The focused results in the azimuth invariant and variant cases are shown in Fig. 2 (a) and Fig. 2(b), respectively, where the corresponding ground range of the focused point targets is denoted on the top of the Fig. 2.

The impulse responses analyses of the point targets A and B in azimuth invariant and variant cases are shown in Fig. 3 and Fig. 4, respectively. It could be seen from Figs. 3–4 that PT A located at the

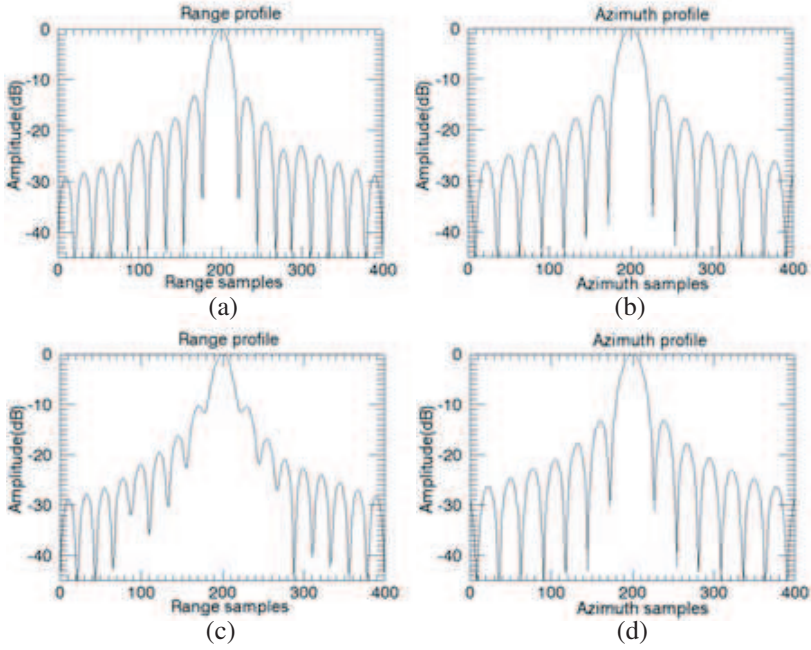

Figure 3. Point target analysis in azimuth invariant case. (a) Range profile and (b) azimuth profile of the focused point target A. (c) Range profile and (d) azimuth profile of the focused target B. (1 range pixel = 0.083 m, 1 azimuth pixel = 0.024 m).

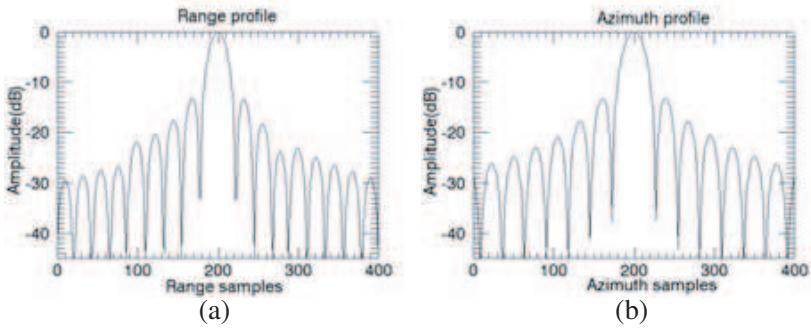

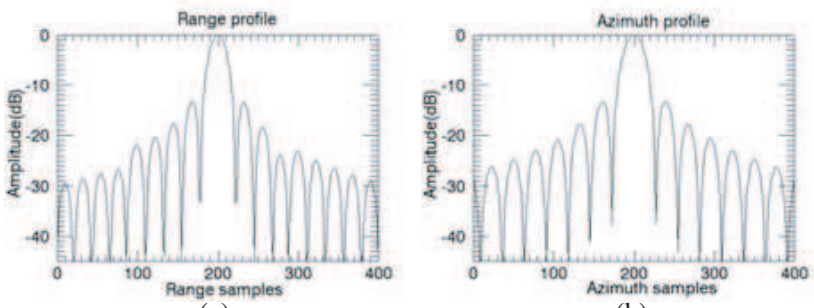

Figure 4. Point target analysis in azimuth variant case. (a) Range profile and (b) azimuth profile of the focused point target A. (c) Range profile and (d) azimuth profile of the focused target B. (1 range sample = 0.083 m, 1 azimuth pixel = 0.023 m).

scene center is well focused while PT B is noticeably degraded. The degraded image quality of PT B is due to the application of the range-invariant SRC filter. If we restrict the quadratic phase error (QPE) in SRC within $\pm\frac{\pi}{2}$, the algorithm can handle a range invariance region of 1259.8 m in the azimuth invariant case and 1264.2 m in azimuth variant case.

6. CONCLUSION

A new RDA is developed in this paper based on a bistatic point target spectrum, i.e., the improved LBF. The spectrum has an analogous analytical expression with the monostatic point target 2-d spectrum and is more accurate than original ELBF. The ILBF spectrum is expanded to the third order to implement the new RDA. The new algorithm has a simpler formulation than existing bistatic RDA and is able to cope with moderate high squint data. Both the azimuth invariant and variant bistatic SAR modes are simulated. Simulation results have validated our approach.

REFERENCES

1. Sun, J., S. Mao, G. Wang, and W. Hong, "Extended exact transfer function algorithm for bistatic SAR of translational invariant case," *Progress In Electromagnetics Research*, Vol. 99, 89–108, 2009.
2. Wu, J., J. Yang, Y. Huang, Z. Liu, and H. Yang, "A new look at the point target reference spectrum for bistatic SAR," *Progress In Electromagnetics Research*, Vol. 119, 363–379, 2011.

3. Sun, J., S. Mao, G. Wang, and W. Hong, "Polar format algorithm for spotlight bistatic SAR with arbitrary geometry configuration," *Progress In Electromagnetics Research*, Vol. 103, 323–338, 2010.
4. Mao, X., D.-Y. Zhu, and Z.-D. Zhu, "Signatures of moving target in polar format spotlight SAR image," *Progress In Electromagnetics Research*, Vol. 92, 47–64, 2009.
5. Nie, X., D.-Y. Zhu, and Z.-D. Zhu, "Application of synthetic bandwidth approach in SAR polar format algorithm using the deramp technique," *Progress In Electromagnetics Research*, Vol. 80, 447–460, 2008.
6. Wang, X., D. Y. Zhu, Z. D. Zhu, "An implementation of bistatic PFA using chirp scaling," *Journal of Electromagnetic Waves and Applications*, Vol. 24, No. 4-5, 447–460, 2010.
7. Loffeld, O., H. Nives, et al., "Models and useful relations for bistatic SAR processing," *IEEE Transactions on Geoscience and Remote Sensing*, Vol. 42, No. 10, 2031–2038, 2004.
8. Neo, Y. L., F. H. Wong, et al., "A two-dimensional spectrum for bistatic SAR processing using series reversion," *IEEE Geoscience and Remote Sensing Letters*, Vol. 4, No. 1, 93–96, Jan. 2007.
9. Wang, R., O. Loffeld, et al., "A bistatic point target reference spectrum for general bistatic SAR processing," *IEEE Geoscience and Remote Sensing letter*, Vol. 5, No. 3, 517–521, 2008.
10. Natroshvili, K. and O. Loffeld, "Focusing of general bistatic SAR configuration data with 2-D inverse scaled FFT," *IEEE Transactions on Geoscience and Remote Sensing*, Vol. 44, No. 10, 2718–2727, Oct. 2006.
11. Li, F., S. Li, and Y. Zhao, "Focusing azimuth-invariant bistatic SAR data with chirp scaling," *IEEE Geoscience and Remote Sensing letters*, Vol. 5, No. 3, 484–486, Jul. 2008.
12. Neo, Y. L., F. H. Wong, and I. G. Cumming, "Focusing bistatic SAR data using the nonlinear chirp scaling algorithm," *IEEE Transactions on Geoscience and Remote Sensing*, Vol. 46, No. 9, 2493–2505, 2008.
13. Neo, Y. L., F. H. Wong, and I. G. Cumming, "A comparison of point target spectra derived for bistatic SAR processing," *IEEE Transactions on Geoscience and Remote Sensing*, Vol. 46, No. 9, 2481–2492, 2008.
14. Wang, R., O. Loffeld, et al., "Extending Loffeld's bistatic formula for the general bistatic SAR configuration," *IET Radar, Sonar & Naviga.*, Vol. 4, No. 1, 74–84, 2010.